Journal of Visualization, Vol. 8, No. 4 (2005) 287

Visualization of Flows in the Gap between Concentric Cylinders

Ait Aider, A. [1)]

1) Département de Mécanique, Université Mouloud Mammeri BP 17 RP Tizi Ouzou, Algérie.

Visualization of flows produced in a concentric cylinders system is made with Kalliroscope. When the system is closed (Fig. 1) and the inner cylinder rotating, the natural transition observed from the basic Couette flow to turbulent flow is as reported on the photographic sequence of Fig. 3: Taylor vortex flow → wavy vortex flow → modulated wavy vortex flow → weak turbulence. When the system is azimuthally opened (Fig. 2), and both cylinders are at rest, the main transitional sequence of the Dean flow subsequent to a basic Poiseuille flow is reported on Fig. 4; when the basic flow is a combination of Couette and Poiseuille flows, observations made at the inlet, the core and the outlet of the subsequent Taylor-Dean flow, show (Fig. 5) that different flow patterns develop themselves simultaneously.

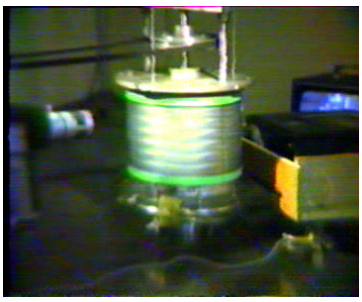

Fig. 1. Closed Taylor-Couette system.

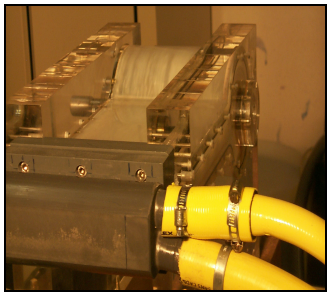

Fig. 2. Open Taylor-Dean system.

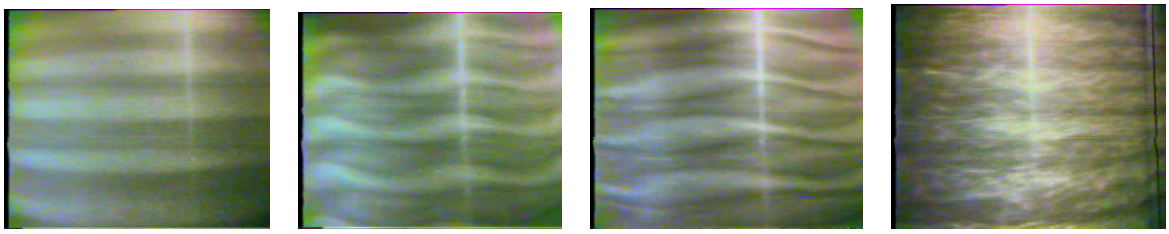

Fig. 3. The main transitional sequence of the closed Taylor-Couette flow.

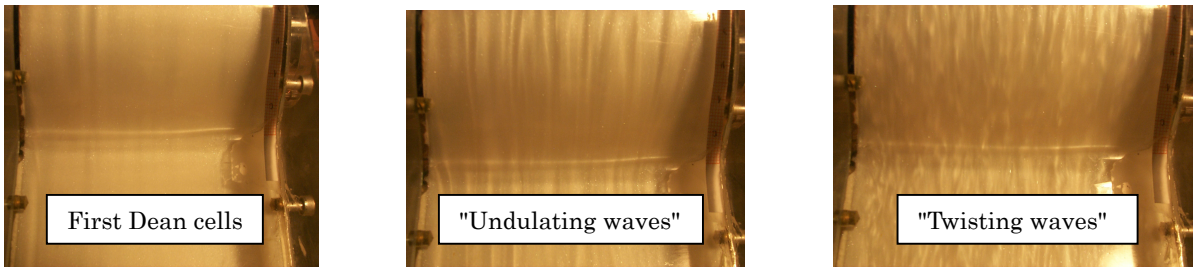

Fig. 4. The main transitional sequence of the Dean flow.

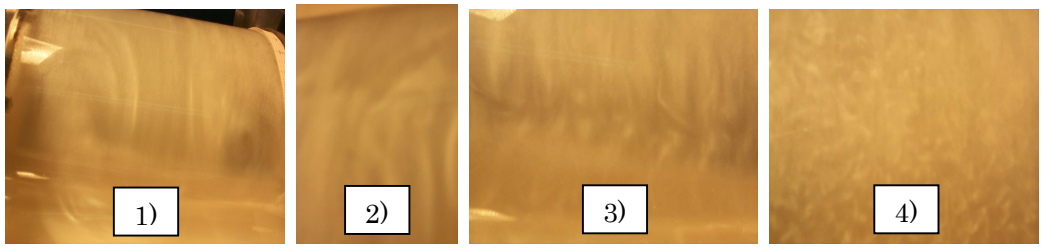

Fig. 5. Taylor-Dean flow : structures observed at 1) the entry, 2) the core, 3) the exit, 4) stochastic flow in the core.

Visualization of Buoyancy Opposing Flow Structures in a Small Length Scale Fluidic Junction

Walsh, P. A. 1), Davies, M. R. D. 1) and Dalton, T. 1)
1) Stokes Research Institute, University of Limerick, Rep. of Ireland. E-mail: Pat.Walsh@UL.ie

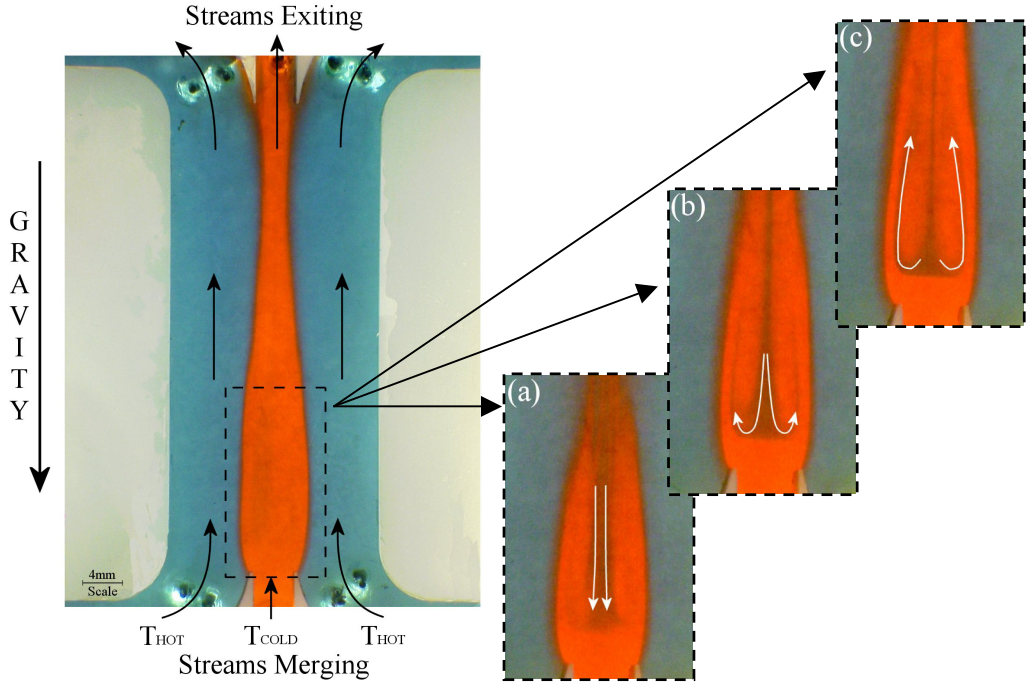

Fig. 1. Laminar Plume structure observed in a small length scale fluidic junction under buoyancy opposing flow boundary conditions. Re of outer streams, 23, Re of center stream, 2.8 and Gr between streams, 688. Also shown are three instantaneous subfigures (a), (b) & (c) of the plume structure developing and indicating the presence of a symmetrical recirculation within the plume.

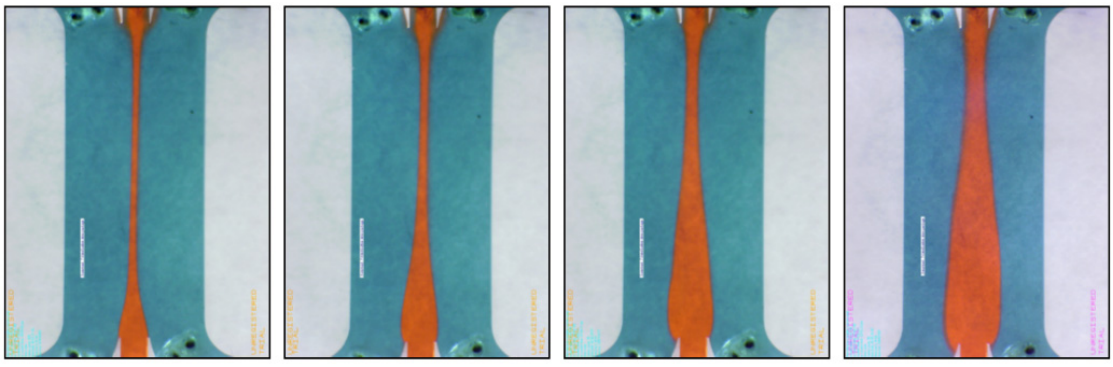

Fig. 2. Visualization images outlining the effect of increasing Grashof number for the same Re boundary conditions as in Fig. 1. Forced viscous flow conditions seen to prevail at low Gr numbers and laminar recirculation zones seen to develop at high Gr numbers. The corresponding Richardson number range for these images is 0.5 to 1.7 from left to right.

The plume structure obtained in a laminar viscous flow regime under buoyancy opposing flow conditions is detailed by means of flow visualization using dyed water streams. The boundary conditions are obtained by raising the temperature of outer streams entering the device above that of the center stream. It is seen that a plume structure is inhibited at low Gr numbers due to a dominant inertia force exerted by the forced outer stream. A laminar plume in the form of a symmetrical recirculation zone develops at higher Grashof numbers due to the equalising and subsequent dominance of buoyancy forces over inertia forces.

Journal of Visualization, Vol. 8, No. 4 (2005) 289

Excited Single-Phase (Liquid) Jets

Milenkovic, R. [1)]***, Sigg, B.*** [2)] ***and Yadigaroglu, G.*** [2)]

1) Laboratorium für Thermohydraulik LTH-PSI, Paul Scherrer Institut, OVGA 415, CH-5232 Villigen PSI, Switzerland.

2) Laboratorium für Kerntechnik, ETH Zentrum CLT-D3, CH-8092 Zürich, Switzerland.

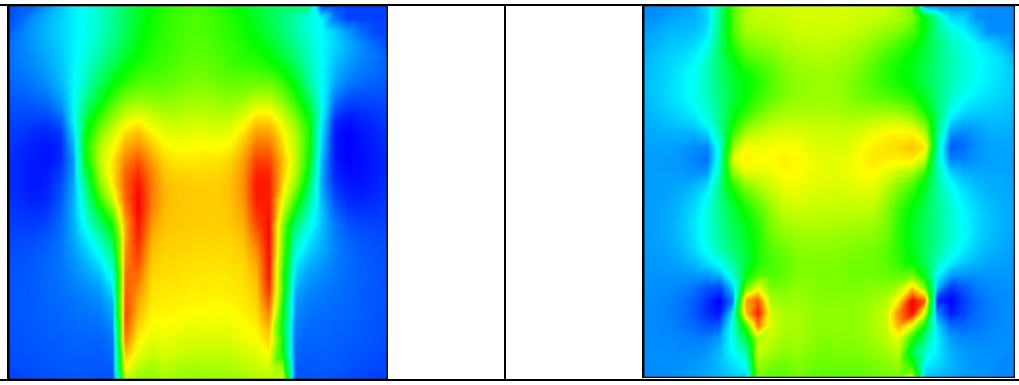

Fig. 1. Phase-averaged vertical velocity component (excitation frequency 1 Hz-left, and 3 Hz-right).

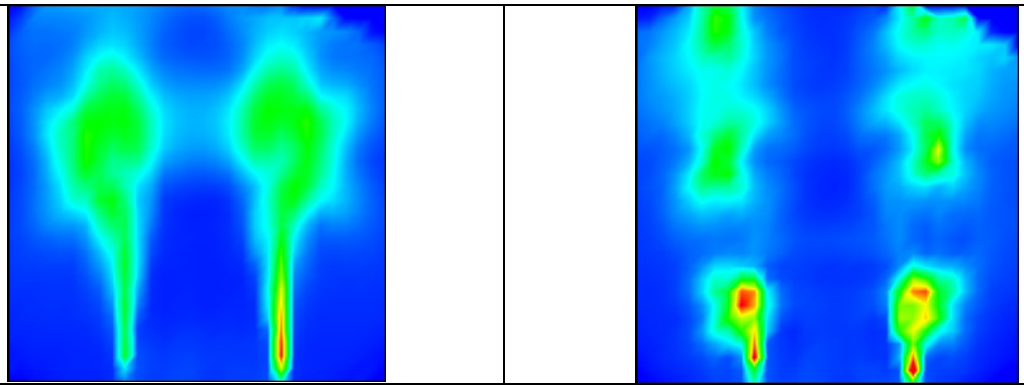

Fig. 2. Phase-averaged standard deviation of the vertical velocity component (excitation frequency 1 Hz-left, and 3 Hz-right).

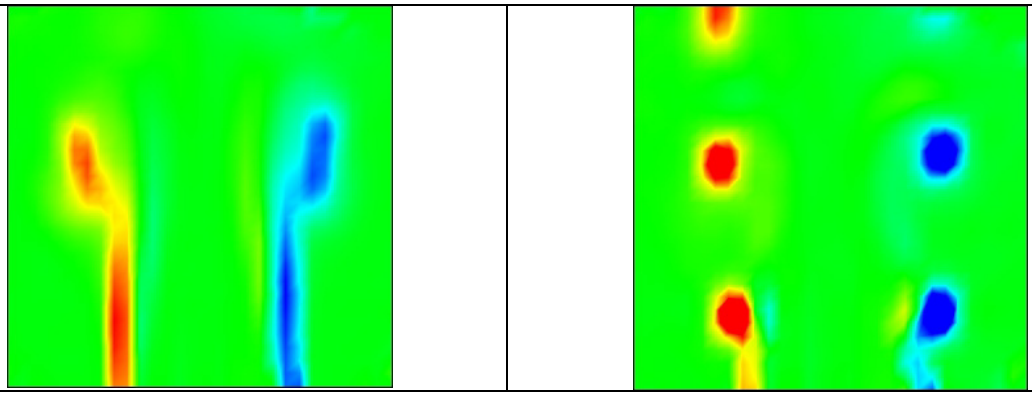

Fig. 3. Phase-averaged azimuthal vorticity component (excitation frequency 1 Hz-left, and 3 Hz-right).

The scalar maps show some phase-averaged quantities obtained by PIV in the developing region of a periodically triggered, axisymmetric liquid single-phase jet. Excitation frequencies are 1 Hz and 3 Hz, corresponding to Strouhal number St = 0.3 and 0.6, respectively. Triggering of the jet shear layer leads to concentration of the shear layer vorticity in the coherent vortex rings which travel downstream at about half of the jet velocity.

Numerical and Experimental Observation of Chaotic Mixing in Microfluidic Mixer

Xia, H. M. [1], Shu, C. [1], Wan, S. Y. M. [2] and Chew, Y. T. [1]

1) Department of Mechanical Engineering, National University of Singapore, 119260, Singapore.

2) Singapore Institute of Manufacturing Technology, 71 Nanyang Drive, 638075, Singapore.

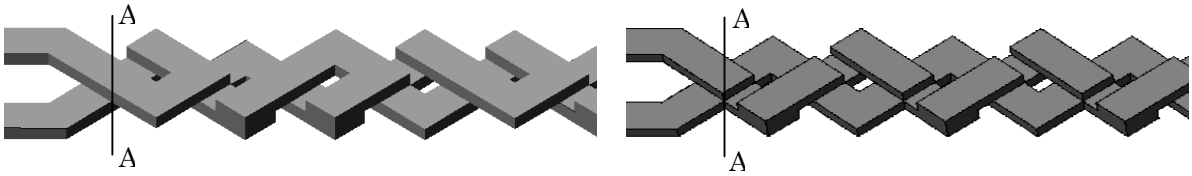

Fig. 1. Schematic of the chaotic mixer structure. Model A (left) and B (right).

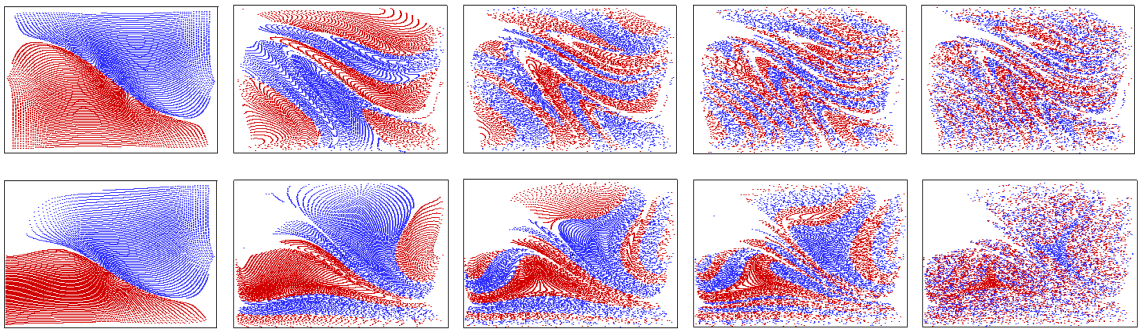

Fig. 2. Inert particle mixing at section A (as indicated in Fig. 1). (top) Model A, Re = 0.02, the first 5 cycles; (bottom) Model B, Re = 0.2, the first 4 cycles and the 10th cycle.

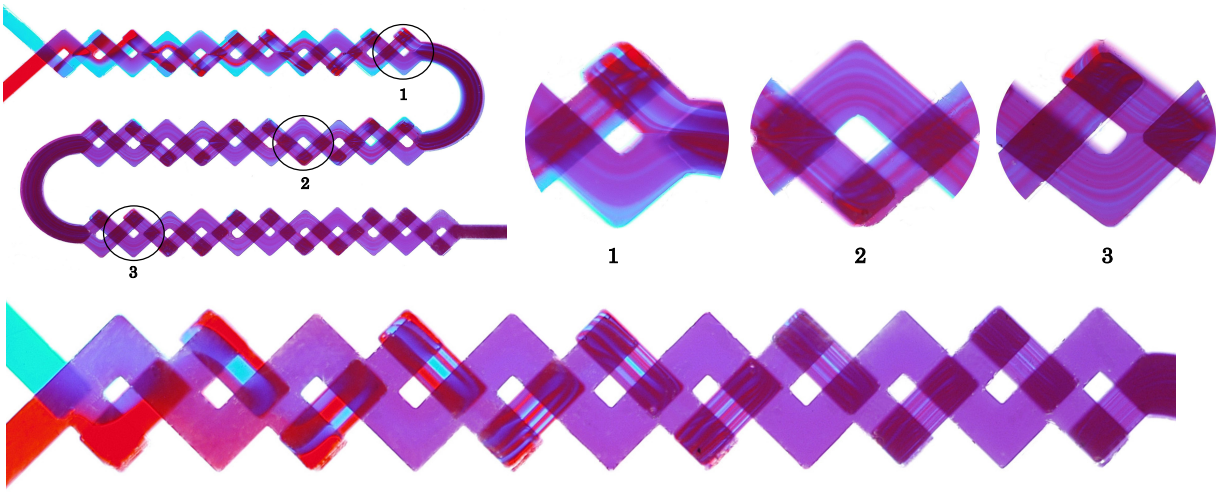

Fig. 3. Experimental mixing pictures with scaled-up model A (top) and model B (bottom) at Re = 0.01. The fluid is highly viscous 98% glycerol-2% liquid food dye (red and blue) solution.

Both the chaotic mixers (Fig. 1) adopt a two-layer overlapping channels structure, which is very efficient for fluid manipulations such as stretching and folding, splitting and recombination. Even at extremely low Re (~10^{-2}), chaotic advection can be generated.

Both particle tracing simulation (Fig. 2) and experimental results (Fig. 3) show that as the fluids are driven through the mixer, striations occur resulting in large interface area to promote diffusive mixing.

Microstructural Finite Element Analysis of Mo-Si-B Alloy in High Temperature Applications

Chollacoop, N. [1], Alur, A. P. [2] and Kumar, K. S. [2]

1) National Metal and Materials Technology Center (MTEC), Pathumthani, Thailand.

2) Division of Engineering, Brown University, Providence, RI, USA.

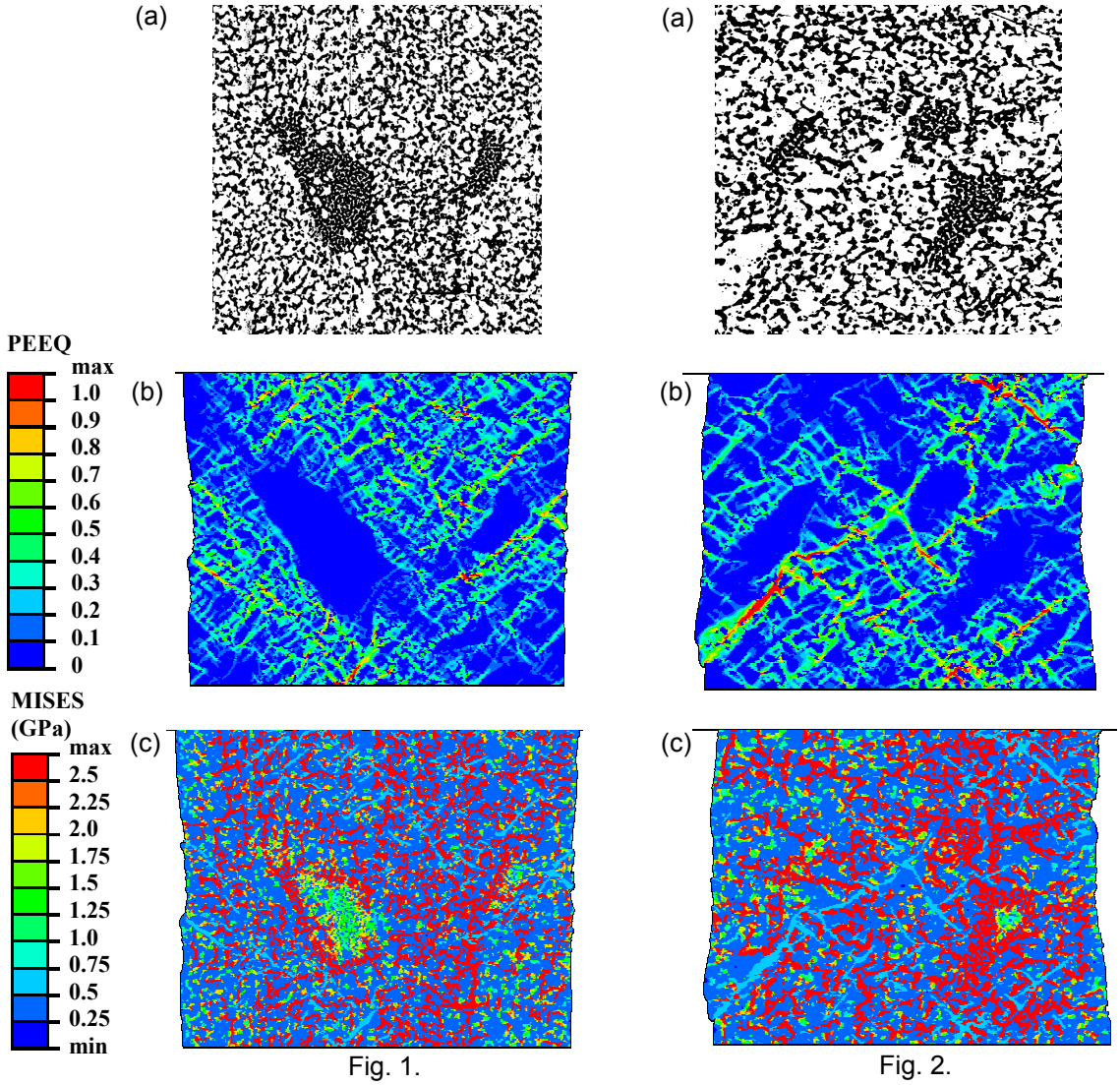

Fig. 1.

Fig. 2.

The optical micrographs of Mo-Si-B alloys showing two (Fig. 1 (a)) and three (Fig. 2(a)) clusters of T2 (Mo_5SiB_2) phase (shown in black) embedded in Mo solid solution (shown in white) were scanned and digitized into finite element simulation of uniaxial compression. The constitutive relations of both phases were obtained from experimental observation at a temperature of 1000 K and a strain rate of 10^{-3} s^{-1}, where T2 phase only deforms elastically. At maximum compression of 10% engineering strain, the contour plots of plastic equivalent strain (PEEQ) and Mises stress are shown in Fig. 1(b) and Fig. 1(c), respectively, for the case of Fig. 1(a); and Fig. 2(b) and Fig. 2(c), respectively, for the case of Fig. 2(a). The plots show the strain localization in Mo solid solution and stress concentration in elastic T2 clusters due to the inability of T2 clusters to plastically deform. Large T2 clusters also shield off the deformation within the enclosed regions. These numerical findings were well correlated with experimental observation of cracking by the T2 particles in the deformed specimens.* Further uses of this microstructural simulation tool to improve the mechanical properties and/or investigate deformation mechanism are suggested.

* Alur, A. P., Chollacoop, N. and Kumar, K. S., High-temperature compression behavior of Mo-Si-B alloys Acta Materialia, 52 (2004) 5571-5587.